Hindawi
Material Design & Processing Communications
Volume 2022, Article ID 7541853, 9 pages
https://doi.org/10.1155/2022/7541853

Research Article

Reduced Coefficient of Friction of Laser Surface Hardened AISI 4130 Steel Substrates

Matheus Rodrigues Furlani,[1] **Sheila Medeiros de Carvalho**,[1] **Rafael Humberto Mota de Siqueira**,[2] **and Milton Sergio Fernandes de Lima**[2]

[1]*Mechanical Engineering Department, Federal University of Espirito Santo, Av. Fernando Ferrari 51, Vitoria ES 29075-910, Brazil*
[2]*Photonics Division, Institute for Advanced Studies, Trevo Amarante 1, Sao Jose dos Campos, SP 12228-001, Brazil*

Correspondence should be addressed to Sheila Medeiros de Carvalho; sheila_mcarvalho@yahoo.com.br

Received 19 January 2022; Revised 21 February 2022; Accepted 22 February 2022; Published 17 March 2022

Academic Editor: Enrico Salvati

AISI 4130 steels have been used in several engineering applications, although presenting limited hardenability in conventional heat treatments. This contribution is aimed at determining the final hardness and reciprocating wear coefficient of friction (COF) after a given laser surface treatment (LST) with or without a carbon coating (C). The results indicated that the bare (B, without coating) condition produced a deeper case depth as a result of the carbon-rich plasma shielding. The observed microstructural features in the cases B and C showed martensite transformation and cementite formation; the latter is entirely in the C condition. Simple calculations using Rosenthal's formalism indicate a high cooling rate, estimated as $32'280^{\circ}$C/s 40 μm below the irradiated surface and a heat-affected zone bounded by the austenite locus. The hardness near to the surface was higher in case C than in case B, but the overall final hardness is more pronounced when the surface is bare (B) due to plasma shielding. On the other hand, the final COF was very low in the C case (0.1) compared to the B condition (0.6).

1. Introduction

AISI 4130 grade steels are known as medium carbon low-alloy steels, which acquire high mechanical strength according to a given heat treatment. This alloy is widely used in aerospace and petrochemical applications because of its ultrahigh tensile strength, while it has excellent fabricability and weldability in the annealed condition. However, AISI 4130 steel has limited hardenability, which limits its use when wear conditions are excessive. According to the literature [1], wear and corrosion have been pointed out as the main failure modes in AISI 4130 components, particularly in petrochemical plants.

Nowadays, laser surface treatment (LST) is a viable route to alter the tribological conditions of the steel surface, without altering the desirable properties of the component's volume [2]. In this way, a particular part can be machined and welded in the as-received condition and then heat treated to obtain a certain surface property. In most cases, LST does not change the dimensions of the solid and thus is usually called a near-net shape method.

Laser surface treatment (LST) is a technique in which a light source originating from a laser is concentrated in a small region of the material surface, in order to produce a given phase transformation [3]. The continuous movement of the laser beam in a certain direction causes a transformation of a line (a laser track), while several adjacent lines allow treating an entire surface. The literature [4] reports the use of lasers for surface hardening (martensitic transformation), surface remelting, and cladding. These LST methods bring advantages compared to traditional methods due to automation, speed, and low heat input (less distortion and warping) [5]. The present method uses LST to partially remelt a layer of an AISI 4130 steel plate with and without graphite on its surface.

This study is aimed at determining the hardness and coefficient of friction obtained after LST of medium carbon low-alloy steel. However, as one of the problems pointed

Table 1: Chemical composition of the AISI 4130 bars.

C	Si	Mn	P	S	Cu	Cr	Ni	Mo	W
0.280	0.29	0.80	0.007	0.01	0.10	1.00	0.15	0.25	0.0038
V	Nb	Co	Al	Sn	As	Sb	N	H_2	Fe
0.026	0.0026	0.01	0.022	0.008	0.006	0.0026	0.0043	0.00014	Balance

out in the state of the art is the issue of decarburization [6], the LST of AISI 4130 steel parts in which there is, or not, a graphite surface layer will be compared from the point of view of these two mechanical behaviors.

Moradi et al. [7] have already studied the laser hardening of AISI 4130 steel using a diode laser beam. Depending on the experimental conditions, these authors obtained a maximum penetration of 1.3 mm and a maximum hardness of just under 800 HV. According to the authors, melting can be avoided and the microstructure was predominantly martensitic. In another publication [8], these authors showed that the deposition of a carbon layer on the surface of the AISI 4130 steel part improves the laser beam absorption and the hardness of the martensitic layer.

Casalino et al. [9] reported a case depth of about 0.3 mm in an AISI 4130 steel plate using a pulsed mode Nd:YAG laser beam. In this case, some liquid intervention appeared near to the irradiated surface, which was supposed to decrease the local hardness because of the descarburization phenomenon. These authors also proposed a numerical calculation (finite element method) of the laser hardening with barely good agreement with the experimental results.

Fan et al. [1] studied the tribology of a Fe-based composite layer in AISI 4130 parts. Laser cladding using (1) Fe72.2Cr16.8Ni7.3Mo1.6Mn0.7C0.2Si1.2 and (2) Fe77.3Cr15.8Ni3.9Mo1.1Mn0.5C0.2Si1.2 powders was studied. The corrosion properties of the coated steel parts have been considered improved; however, the wear behavior (in reciprocating sphere tests) is almost the same of the original (bare) base material. The final coefficient of friction (COF) for the bare and the optimal parameters for the laser-cladded surfaces were 0.8 and 0.6 for (1) and (2), respectively.

As can be noted in the cited references [1–6], there is a lack of knowledge in the laser surface treatment using a carbon coating to mitigate decarburization and reducing COF, increasing the surface hardness but without changing the volume microstructure.

2. Materials and Methodology

The base materials are AISI 4130 as-annealed cylindrical bars with 12.8 mm diameter segmented in 3 mm thick samples. The chemical composition provided by the fabricant is given in Table 1. The as-received material microstructure is composed of perlite and ferrite with an average hardness of about 220 HV.

Laser surface hardening was carried out using a 2 kW continuous wave fiber laser produced by IPG Co. The focal length was 160 mm with a minimum spot diameter of 100 μm, but the actual radius $\omega(Z)$ depends on the position of the sample surface with respect to the focal plane, as presented in

$$\omega(Z) = \omega_0 \left[1 + \left(\frac{M^2 \lambda . Z}{\pi . \omega_0^2}\right)^2\right]^{1/2}, \quad (1)$$

where Z is the distance from the focal plane, ω_0 is the minimum beam radius, M^2 is the beam quality factor, and λ is the laser wavelength. Here, $Z = 12.2$ mm, $\omega_0 = 50$ μm, and $\lambda = 1.080$ μm. The laser beam quality was measured in our labs giving a value of M^2 as nine. In the current case, $Z = -4$ mm and $\omega = 0.25$ mm.

The sample moving was realized by a CNC table. The table moves at a constant velocity from 1 to 160 mm/s and could be programmed to any direction in an area of 430 × 500 mm^2. The Z-axis is also computer controlled with a 1 μm step resolution and is used to change the focal distance Z (equation (1)). To process the entire surface, the laser beam moved in a square zigzag with partial superposition between each track. The lateral shift between each laser track was 0.5 mm, and as the beam diameter was estimated (equation (1)) as 0.5 mm, the theoretical superposition between each laser track was zero. Ten-second delay was fixed between one track and another to avoid overheating. After some optimization of the process parameters, the scanning speed was fixed at 10 mm/s and the laser beam power was 150 W. When the heat input (HI), i.e., the ratio power/speed, was higher than 15 J/mm, the surface damage was severe. On the other hand, when HI < 15 J/mm, the surface seemed unchanged.

The samples were surface processed in ambient conditions, i.e., without protective gas shielding. To access the effect of the surface condition, two types of samples were considered: B-bare base material was just grounded with a SiC600 paper and C-coated (coated with a graphite layer) after grinding. The thickness of the graphite layer was approximately 10 μm, as evaluated by the scotch method; however, this value could change due to the manual spray procedure.

The metallography has been done using standard cutting, grinding, and polishing methods, and the chemical etching was nital 2% (2% nitric acid in ethanol). The light optical microscope is a Zeiss Imager2.M equipped with a camera.

To determine the phases present on the laser-treated surfaces, X-ray diffractometry (XRD) was used. The Rigaku equipment, Ultima IV model, was operated at 40 kV and 20 mA in the Bragg-Bretano configuration and using a copper anode. The samples were rotated during measurements to decrease the texture effects on the X-ray peak intensities. The peak analyses were performed using the Crystallography Open Database [10].

The evolution of temperature as a function of depth was estimated using the Rosenthal formalism [11], which proved

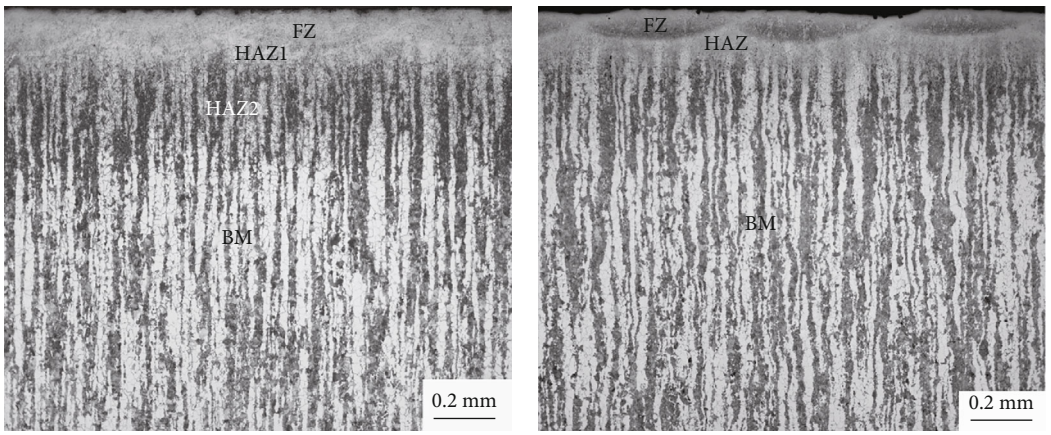

(a) (b)

Figure 1: Light optical micrographies of the samples' cross section near to the treated surfaces: (a) belongs to the material processed on the original condition (B-bare) and (b) belongs to the surface that received a layer of graphite before LST (C-coated).

(a) (b)

Figure 2: Photographs of two moments during the laser processing: (a) without coating and (b) with a C-coating. The effect of the surface state on the plasma glow could be perceived comparing (a) to (b).

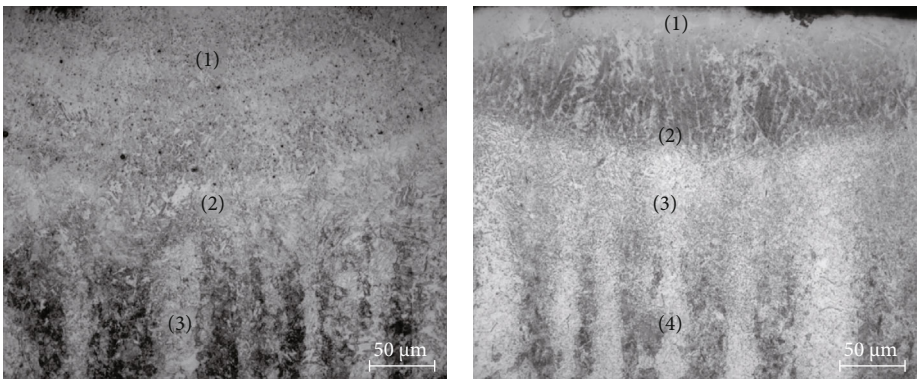

(a) (b)

Figure 3: Light optical micrographies of the samples' cross section bearing to the treated surfaces: (a) B-bare condition and (b) C-coated condition. More magnification from Figure 1.

to be good enough to reproduce conduction welding regimes [12]. The energy absorbed during laser beam heating is mainly from the heat conduction dissipated to the solid volume; thus, the temperature field could be calculated from the heat diffusion equation. Rosenthal's solution proposes a point heat source at constant velocity, V, over a semi-infinite solid with axial origin at the intersection of the laser beam axis with the material surface. The model assumes constant and isotropic thermal properties (conductivity and specific heat) and negligible latent heat. The steady-state temperature distribution of a moving source is then given by

$$T(x, y, z) = T_0 + \frac{\beta P}{2\pi k r} \operatorname{Exp}\left[-\frac{V}{2\alpha}(x + r)\right], \quad (2)$$

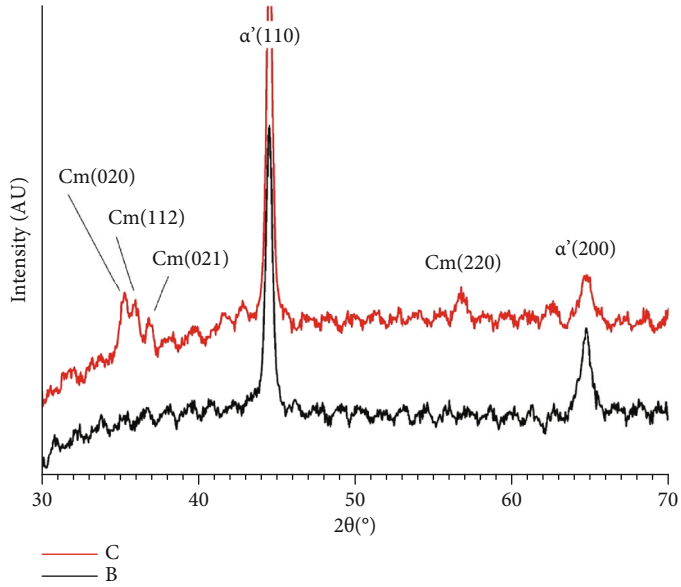

FIGURE 4: X-ray diffraction spectra of the LST under conditions B and C. The phases martensite (α') and cementite (Cm) are presented together with the Miller indices.

where T_0 is the ambient temperature, β is the laser-matter absorptivity, P is the laser power, k is the thermal conductivity, and α is the thermal diffusivity. The radius (r) considers a given point of interest in a Cartesian space. For the present case, the material constants in equation (2) are [13] $k = 46\,\mathrm{W} \cdot \mathrm{m}^{-1} \cdot \mathrm{K}^{-1}$ and $\alpha = 1.2 \times 10^{-5}\,\mathrm{m}^2\,\mathrm{s}^{-1}$, and the liquidus temperature is 1510°C.

The microhardness tester is Future-tech FM 700 equipment using a Vickers pyramid and loads from 5 to 500 gf. Here, the applied load was 100 gf and the dwell time was 10 s.

Reciprocating sliding wear tests were carried out using a TRB3 equipment (Anto-Paar) using a 3 mm diameter hard metal ball and 2 N normal load under ambient temperature. The scratches presented a full amplitude of 4 mm, with a maximum linear speed of 3 cm/s and a frequency of 2.39 Hz. The tests stopped after the ball travels 70 m or 3655 seconds. The dynamic coefficient of friction (COF) was recorded as a function of time, and the damaged area of the counter body (ball) was evaluated using a light optical microscope and ImageJ software. Every surface was tested three times.

3. Results and Discussion

Figure 1 represents two cross-sectional images through the laser-treated samples with a defocused beam with a diameter of 0.5 mm, a processing speed of 10 mm/s, and a laser beam power of 150 W. The metallography cuts were performed in such a way to show a cut 90° from the beam scanning direction. Thus, semielliptical liquid baths are visible (Figure 1) in the so-called fusion zone (FZ), the base material (BM) marked by dark pearlite and light ferrite, and an intermediate region called the heat-affected zone (HAZ), which could be spliced in HAZ1 and HAZ2 as shown in Figure 1(a). The subzone HAZ2 contrasted with BM because of a distinctive dark etch.

Figure 1(a) belongs to the material processed on the original sanded surface (B-bare) and Figure 1(b) to the surface that received a layer of graphite (C-coated). Although it is estimated that the C-coated surface has a greater absorbance to the laser beam [5] and, consequently, a greater amount of liquid should be formed, this was not observed. The maximum depth of the FZ is slightly lower in case C compared to case B, i.e., 0.09 mm and 0.12 mm, respectively. As the only difference between conditions B and C is in the surface composition, there is a heat input reduction effect in case C compared to case B. Experimentally, there is a large difference between plasma luminescence when the sample is coated with graphite (C) or without coating (B), as depicted in Figure 2.

Figure 2 shows two photographs taken at different times of a set of pieces treated together in the laser workstation (got with a cell phone camera). Eight samples are visible, being four at the right uncoated (B) and the other four carbon-coated (C). In Figure 2(a), the laser beam (visible light on a square piece) is moving from left to right with a constant velocity of 10 mm/s. In this case, the plasma associated with the normal air treatment appears to be confined to a region about 3 mm wide (Figure 2(a)). Continuing to the left, the laser beam hits the carbon-coated sample and the plasma ignites so strongly that it obscures the sample being treated (Figure 2(b)). There is enough plasma to observe the so-called plasma shielding (PS), where the plasma is so dense and absorbs some of the beam's energy [14]. For the exact same laser beam intensity, the plasma expanded more when it strikes the carbon target because its first ionization energy is about 40% lower than that of nitrogen or oxygen [15]. Another source of exothermic heat is the carbon reaction with oxygen, giving a distinctive flame when the beam strikes the sample for the first time. PS is the reason why the fusion depth is greater in condition B compared to condition C (Figure 1). Note that this observation contradicts

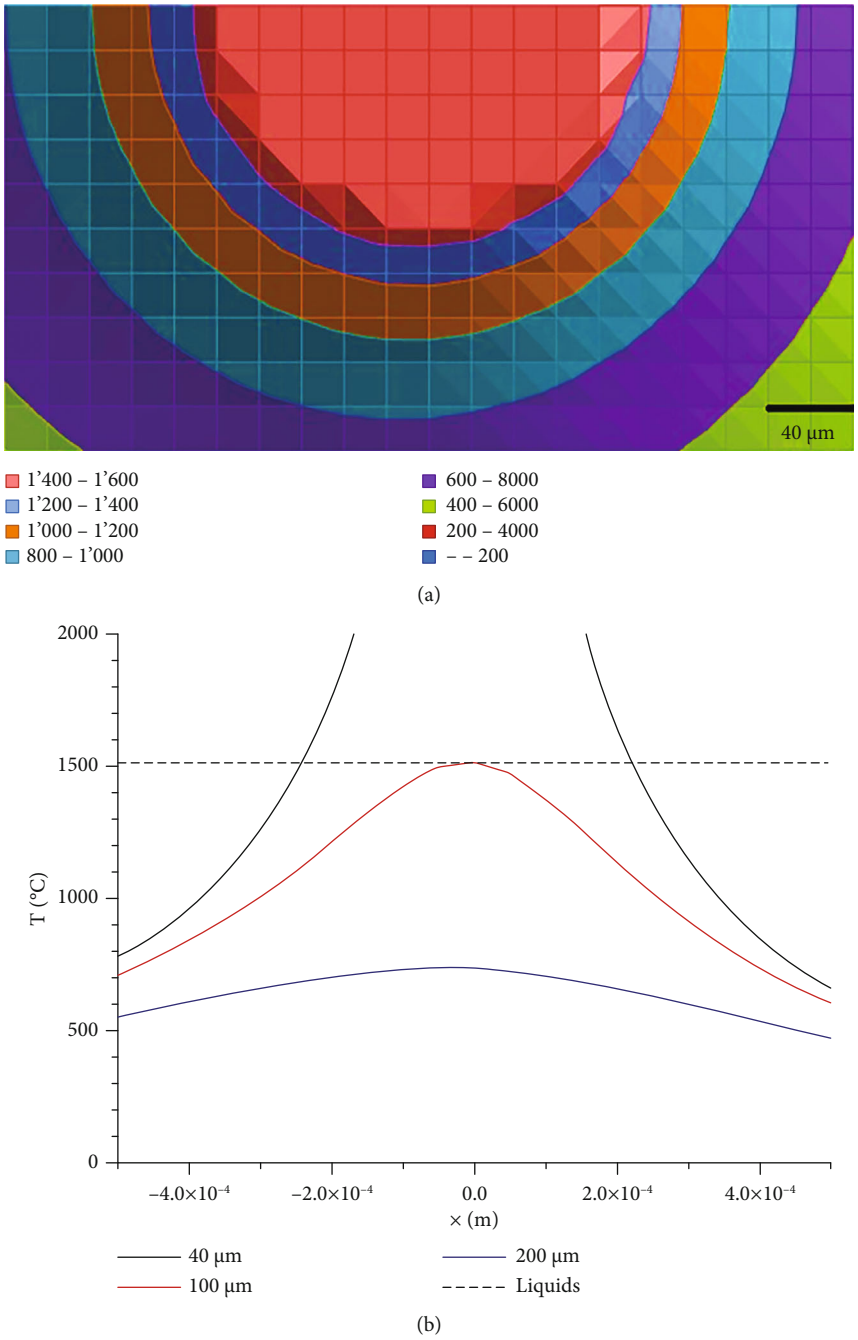

FIGURE 5: Estimated temperature profiles from equation (2) from a transversal cut when the laser beam vector is given by the arrow and $\beta = 30\%$: (a) cross section of steady-state temperature profiles; (b) temperature versus time for a point near to the surface (40 μm), at the interface FZ/HAZ (100 μm) and 200 μm below the treated surface.

some references, such as Ref. [5], in which carbon coating is applied to increase the conversion of light into thermal energy (absorptivity). However, this procedure is typically performed for CO_2 laser beams that have such low absorptivity in the bare condition (Figure 2(a)) that, even with plasma shielding, it is worth applying an absorbing layer.

The microstructures obtained in each case (B and C) are presented with greater magnification in Figure 3. In case B (Figure 3(a)), there are three numbers indicating (1) fusion zone (FZ), (2) heat-affected zone 1 (HAZ1), and (3) heat-affected zone 2 (HAZ2). The dendritic structure of FZ has some dimples due to chemical etching with nitric acid. Both regions (1) and (2) are marked by martensitic structures, although it is possible to distinguish the allotriomorphic ferrites in (1). These findings are similar to those reported by Neto et al. [16] using arc and laser welding procedures in AISI 4130 samples. In Figure 3(a), the transition between (2) and (3) is tenuous, but some martensite could be seen close to the original pearlite veins (dark microconstituent in Figure 3(a)). The

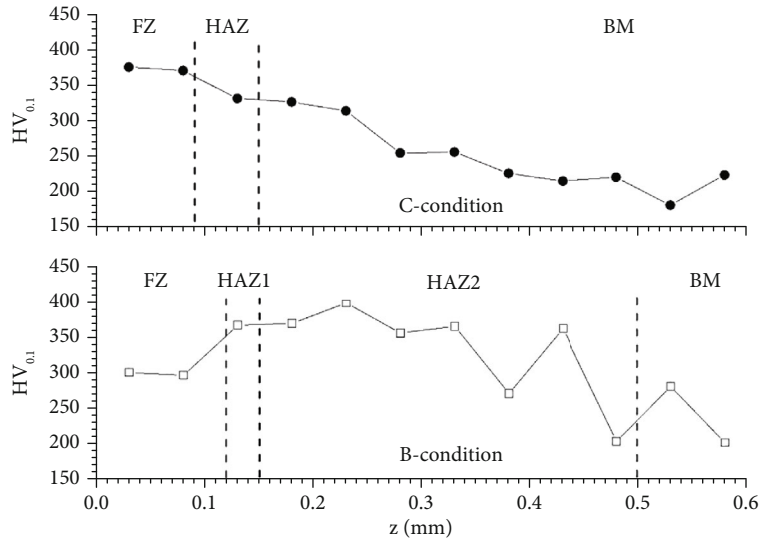

Figure 6: Vickers hardnesss of the samples (cross section). The ordinate origin corresponds to the free surface exposed to the laser treatment under B (base) and C (coated) conditions. The vertical lines correspond approximately to the fusion zone (FZ), heat-affected zone (HAZ), and base material (BM).

HAZ2 (3) is characterized by a partial martensitic transformation of the original microconstituents (pearlite and ferrite).

In the case of the sample in condition C (Figure 3(b)), there are four numbers: (1) the free surface region, with a white top layer usually associated with the cementite formation; (2) FZ with dark dendrites and allotriomorphic ferrite; (3) a HAZ marked by solid-state martensitic transformation; and (4) a region similar to HAZ2 in the B condition. The FZ of case C ("(2)" in Figure 3(b)) is slightly darker than that of case B for the same etching time, perhaps because some carbon is diluted in the FZ. Another open question is the possible formation of cementite in position (1) of Figure 3(b), as a large portion of carbon vanished from the surface during LST.

The LST surfaces were studied by XRD to obtain the phases. Not surprisingly, the as-LST substrates are marked by hematite and magnetite (iron oxides) which will not contribute to the mechanical behavior. Therefore, to avoid these peaks, the surfaces were cleaned using 3M Scotch-Brite and a detergent solution followed by abundant water rinsing. Figure 4 shows two XRD spectra referring to surfaces treated with (C) and without (B) graphite coating. The peaks referring to the martensite (α') and cementite (Cm) phases, with the respective Miller indices, were included for comparison. Note that the martensitic phase is observed in both conditions B and C, while cementite is only visible in C. This shows that a part of the carbon on the surface of the C-sample reacted to form this carbide. The baseline wave in both cases was due to the spin of the sample during the diffractometry and was associated with the periodic pattern that the laser beam prints on the surface of the material. The background peaks refer to the moment when the X-ray wavefront illuminates the surface in the same direction as the LST marks. The valleys are coincident with an irradiation lateral to the LST marks, with fewer crystal structures being diffracted.

As the FZ and HAZ dimensions were too small to experimentally determine the temperature profiles as a function of time, numerical calculations were performed based on the Rosenthal formalism (equation (2)). An unknown variable, the absorptivity (β), was considered accordingly to the FZ dimensions of Figure 1. As explained before, due to plasma shielding (Figure 2) the absorptivity in B and C cases were different, giving a value of $\beta = 0.32$ (B) and 0.28 (C), respectively. For clearness purposes, it was set $\beta = 30\%$ for the current calculations. Figure 5(a) is a section of a temperature versus x-direction (equation (2)) at the centerline when a laser beam moves to the left. The FZ is represented by a large red area in the top-middle and the other temperature ranges are listed on the left. Comparing Figure 5(a) and Figure 3, it can be assumed that HAZ was contained in a temperature range between 1400 and 800°C, which is approximately the range between solidus and A3 temperatures of the Fe-C phase diagram [17]. Evidently, this is only an estimate due to the wide temperature range shown in Figure 5(a) and due to the composition of the alloy under study. However, it could be estimated that the austenite *locus* effectively bounds the HAZ where martensite was present. At the interface between HAZ2 and BM (Figure 1(a)), the estimated temperature was around the intercritical temperatures of the steel [12]. However, the absence of a clear HAZ2/BM interface in Figure 1(b) (C-coated) indicated that the plasma shielding is apposite to reduce the heat input into the material volume.

Figure 5(b) presents the temperature profiles as a function of the distance from a given node of the calculations obtained on the same axis of the laser beam, but at depths of 40, 100, and 200 μm. As seen in Figure 5(a), the laser beam moves towards the left. The low speed of treatment

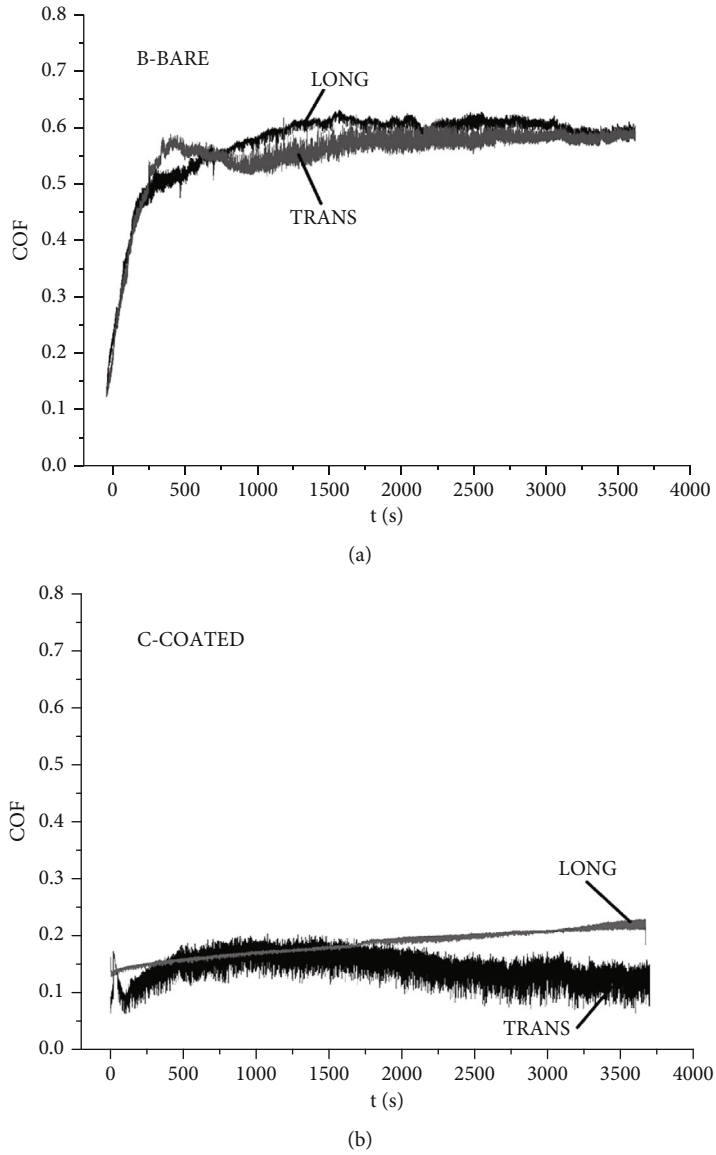

Figure 7: Coefficient of friction as a function of the test time for the B-bare (a) and C-coated (b) conditions considering that the reciprocating movement was longitudinal or transversal to the laser scan lines.

Table 2: Measured wear of the ball after the reciprocating wear test.

mm^2	B-bare	C-coated
LONG	0.063 ± 0.007	0.04 ± 0.02
TRANS	0.09 ± 0.02	0.128 ± 0.002

(10 mm/s) makes the heating and cooling profiles only slightly different at the left or right. Considering an isotherm at 1000°C, the cooling rates at 40 and 100 μm were 32'280 and 21'434°C/s, respectively. These rates are high enough to inhibit any long-range diffusional phase transformation, which promotes martensite formation [18]. However, as seen before, there was a small fraction of allotriomorphic ferrite in the FZ, both in condition B and in C. This ferrite must be a residue of the original BM that did not have time to dissolve in the austenitic matrix. This is because the heating and cooling times are very short. Considering the ordinate axis in Figure 5(b) as the time now, the period where the 40 μm curve is above liquidus is only 0.04 seconds. Another possible source of ferrite was the partial reheating of a zone previously treated by the neighboring laser track. In this case, the white phase could be considered tempered martensite. However, as explained before, the partial superposition of the laser-treated track was set as zero, and thus, the reheating was very limited. Still observing the evolution of the temperature 200 μm below the surface (Figure 5(b)), there seems to be no thermodynamic potential for any phase transformation in a predominantly ferritic-pearlite substrate (BM).

Figure 6 represents the Vickers hardness ($HV_{0.1}$) profile measured from the surface ($z = 0$) for cases B and C. The approximate limits between the different zones, according to Figure 1, are also shown in the figure. The hardness

observed in the FZ of sample C is higher than that observed in sample B due to the dissolution of a portion of carbon (C case) and decarburization (B case). From HAZ1 to HAZ2, the average hardness of the sample in condition B is higher than that in C. According to the assumptions of this study, plasma shielding was responsible for decreasing the heat input into the C condition substrate. A greater amount of heat formed a high volumetric fraction of martensite in HAZ1 and HAZ2 of sample B; however, the hardenability started to drop for $z > 0.4$ mm. From this point, the wide range of hardnesses in HAZ2 in case B compared to C was due to the partial austenitization of the prior pearlite constituent [19]. The cementite layer, as observed in Figure 3(b), was too thin to be indented, although its high hardness could be expected to play a role in reciprocating wear tests.

The coefficient of friction (COF) was measured for the surfaces in the conditions B and C, as shown in Figure 7. Although the surface has been tested three times in the same condition, only one curve is presented for clearness. As the laser treatment produces textures oriented in the beam scanning direction, measurements were taken where the sphere moved longitudinally (LONG) or transversely (TRANS) to the surface marks. In the case of the bare surface (B) (Figure 7(a)), the COF started at about 0.13 and grown rapidly when there was a settlement between the substrate (LST surface) and the counter body (sphere). In the B-TRANS case, there was a COF peak in about 300 seconds, due to the peak breakage of the resolidified material. After that time, the COF dropped slightly until it reached a steady state of about 0.6. When the sphere displacement followed the texture direction as LONG, the peak was not observed, but the final COF was also around 0.6.

When the material was covered with graphite prior to the treatment (C case), the COF was clearly lower than in case B. In Figure 7(b), the test started at a low COF value (~0.07) and remained equal to or less than 0.2. A peak was also noticed when surface C was worn across the treatment lines (TRANS); however, its height and width were much smaller than those in case B (Figure 7(a)). The TRANS condition (Figure 7(b)) presented a final COF of about 0.1, being even smaller than LONG. This result indicates that a part of the resolidified material remained until $t = 3655$ seconds (the end of the test) due to its higher hardness (Figure 6). The current COF (Figure 7(b)) was much smaller than that reported by Fan et al. in a coated and LST AISI 4130 surface [1] and similar to those reported by Aktas et al. [20] for pack-borated Hardox 450 steels. Moreover, the COF results showed a clear advantage in the application of the graphite layer (condition C), regardless of the test direction being longitudinal or transversal to the treatment lines.

At the end of the test, it is common to observe the worn surface to see how much material was lost during the test. However, measuring this quantity in a laser-textured material is very difficult, as its roughness can shift over the wear track. Thus, Table 2 presents an estimate of the worn area on the counter body (hard metal sphere). The usefulness of this measure is in evaluating the damage of the treatment to a given surface under the test conditions reported here. Note that the wear on the sphere when the displacement was longitudinal (LONG) to the treatment lines is situated at 0.06 and 0.04 mm^2 for the conditions B and C, respectively. Considering the estimated error, LONG wear is equivalent, regardless of the condition prior to treatment. However, when the displacement is done transversely to the treatment, the values of the worn area on the sphere rose to 0.09 and 0.128 mm^2, for the conditions B and C, respectively. This increase indicates that the asperities act strongly on ball wear when contact became intermittent.

4. Conclusions

The present work showed that it is possible to perform a laser surface hardening with a reduction in the coefficient of friction (COF) for an AISI 4130 steel plate.

Two surfaces were considered: one grounded and the other on which a layer of graphite was deposited, called bare (B) and coated (C), respectively.

The microstructure of the fusion zone (FZ) and the heat-affected zone (HAZ) was fundamentally martensitic, with maximum hardness of 300 and 380 HV for cases B and C, respectively. Cementite was also formed on the C-coated LST surface, as could be seen in X-ray diffractometry.

Unlike what is pointed out in the literature, the graphite layer reduces heat input due to the phenomenon of plasma shielding [14].

The COF results showed a clear advantage in the application of the graphite layer (condition C), regardless of the test direction being longitudinal or transversal to the treatment lines. At the end of the test, the COF obtained in cases B and C were approximately 0.6 and 0.1, respectively.

Data Availability

The data could be requested by emailing the corresponding author.

Conflicts of Interest

The authors declare that they have no conflicts of interest.

Acknowledgments

This study was financed in part by the Coordenação de Aperfeiçoamento de Pessoal de Nível Superior-Brasil (CAPES) (Finance Code 001) and the scientific initiation program of Federal University of Espirito Santo (Iniciação Científica–Piic/UFES). Thanks are also due to the São Paulo Research Foundation (FAPESP) for the grant nos. 2019/25229-7 and 2016/11309-0.

References

[1] L. Fan, H. Y. Chen, Y. H. Dong, L. H. Dong, and Y. S. Yin, "Wear and corrosion resistance of laser-cladded Fe-based composite coatings on AISI 4130 steel," *International Journal of Minerals, Metallurgy, and Materials*, vol. 25, no. 6, pp. 716–728, 2018.

[2] M. S. F. Lima and F. A. Goia, "Surface hardening of an AISI D6 cold work steel using a fiber laser," *Journal of ASTM International*, vol. 8, no. 2, article JAI103210, 2011.

[3] E. Almeida, "Surface treatments and coatings for metals. A general overview. 1. Surface treatments, surface preparation, and the nature of coatings," *Industrial & Engineering Chemistry Research*, vol. 40, no. 1, pp. 3–14, 2001.

[4] F. Vollertsen, K. Partes, and J. Meijer, "State of the art of laser hardening and cladding," in *Proceedings of the Third International WLT-Conference on Lasers in Manufacturing*, pp. 1–25, AT-Fachverlag GmbH, Fellbach, Germany, 2005, June.

[5] J. Ion, *Laser Processing of Engineering Materials: Principles, Procedure and Industrial Application*, Elsevier, 2005.

[6] W. R. Warke and A. R. Elsea, *The Effects of Decarburization on the Properties of Ultrahigh-Strength Steels (Vol. 154)*, Battelle Memorial Institute, Defense Metals Information Center, 1962.

[7] M. Moradi and M. KaramiMoghadam, "High power diode laser surface hardening of AISI 4130; statistical modelling and optimization," *Optics & Laser Technology*, vol. 111, pp. 554–570, 2019.

[8] M. Moradi, M. K. Moghadam, and M. Kazazi, "Improved laser surface hardening of AISI 4130 low alloy steel with electrophoretically deposited carbon coating," *Optik*, vol. 178, pp. 614–622, 2019.

[9] G. Casalino, M. Moradi, M. K. Moghadam, A. Khorram, and P. Perulli, "Experimental and numerical study of AISI 4130 steel surface hardening by pulsed Nd: YAG laser," *Materials*, vol. 12, no. 19, p. 3136, 2019.

[10] *Crystallography Open Database*http://www.crystallography.net/cod/index.php.

[11] D. Rosenthal, "The theory of moving sources of heat and its application of metal treatments," *Transactions of ASME*, vol. 68, pp. 849–866, 1946.

[12] M. S. F. D. Lima, F. A. Goia, R. Riva, and A. M. D. Espírito Santo, "Laser surface remelting and hardening of an automotive shaft sing a high-power fiber laser," *Materials Research*, vol. 10, no. 4, pp. 461–467, 2007.

[13] Granta Design Ltd, *CES EduPack Software—Material Level 3*, 2013, http://www.grantadesign.com/.

[14] J. M. Vadillo, J. M. Fernández Romero, C. Rodriguez, and J. J. Laserna, "Effect of plasma shielding on laser ablation rate of pure metals at reduced pressure," *Surface and Interface Analysis: An International Journal devoted to the development and application of techniques for the analysis of surfaces, interfaces and thin films*, vol. 27, no. 11, pp. 1009–1015, 1999.

[15] D. R. Lide, "Section 10. Atomic, molecular, and optical physics," in *Ionization potentials of atoms and atomic ions (PDF). CRC Handbook of Chemistry and Physics*, pp. 10–180, CRC Press, 2004.

[16] F. S. Neto, D. Neves, O. M. M. Silva, M. S. F. Lima, and A. J. Abdalla, "An analysis of the mechanical behavior of AISI 4130 steel after TIG and laser welding process," *Procedia Engineering*, vol. 114, pp. 181–188, 2015.

[17] J. Chipman, "Thermodynamics and phase diagram of the Fe-C system," *Metallurgical and Materials Transactions B*, vol. 3, no. 1, pp. 55–64, 1972.

[18] R. A. D. F. Mansur, C. C. D. A. Ferreira, I. Atílio et al., "A comparative study of abbreviated heat treatments for SAE 4130 steel after laser welding," *Materials Research*, vol. 23, no. 4, 2020.

[19] I. Lasota, V. Protsenko, A. Matyushkin, M. Kuznetsov, and S. Gook, "Laser surface hardening of engine camshaft cams," *Materials Today: Proceedings*, vol. 30, pp. 478–482, 2020.

[20] B. Aktaş, M. Toprak, A. Çalık, and A. Tekgüler, "Effect of pack-boriding on the tribological behavior of Hardox 450 and HiTuf steels," *Reviews on Advanced Materials Science*, vol. 59, no. 1, pp. 314–321, 2020.